# Modelling the Behaviour of $UO_{2+x}$ During Melting

M.J. Welland, B.J. Lewis and W.T. Thompson
Department of Chemistry and Chemical Engineering, Royal Military College of Canada
P.O. Box 17000, St. Forces, Kingston, Ont., Canada K7K 7B4

## Abstract

A model is being developed to simulate melting $UO_{2+x}$. The existence of the first order phase change from solid to liquid makes this a moving boundary, Stefan problem. The model presented here numerically solves a system of coupled nonlinear differential equations by the Finite Element Method using commercial software. Included in the treatment are the effects of non-stoichiometry. Material properties at high temperatures are taken from recent published literature. The current model compares well with published experiments. The goal of this research is to model centerline melting in operating CANDU fuel.

## Impetus

Under upset or very high power conditions, particularly with sheath failure, it is possible that the centerline of a fuel pellet will exceed the local melting temperature and begin to melt. This situation is generally avoided in practice. Nonetheless, it is useful to have a fundamental understanding of the melting behaviour of nuclear fuel, should such an incident arise. Since defective fuel rods allow the coolant to come into contact with the fuel, concurrent oxidization by reaction with $H_2O$ or $D_2O$ is also an important consideration.

The introduction of a second phase adds complexity to fuel behaviour models. Models of this type typically require the solution of a set of coupled differential equations in either transient or steady state modes.

Having a change of phase in the material being modelled introduces a boundary at the interface between phases. This boundary moves in time, depending on heat transport and diffusion of phase components. A moving boundary problem is known as *Stefan problem*, and must be treated appropriately. A commonly used technique for modelling Stefan problems is to transform the domain of the problem onto a fixed grid for calculation purposes. This can be accomplished for the general case via the Arbitrary Lagrange Eularian method[1], as is employed in the present work.

## Stefan Problem

In order to derive the equations to model the phase change front, local equilibrium is assumed on either side of the front. In practice, this means that at a specific melting temperature, the concentrations in the adjacent solid and liquid phases are taken directly from the solidous and liquidous lines on the phase diagram. It is assumed that since liquid at the melting temperature is able to crystallize on the adjoining solid, no nucleation time needs to be included. This means that solidification will only occur at a well defined melting front. In the case of constitutional undercooling the combined effect of temperature and concentration on the solidification line, may case a small two-phase region to develop. This is not included in the current model.

The sample of $UO_{2+x}$ is modelled as a solvent of $UO_2$ with a diffusing oxygen solute. In this treatment, $x$ is the stoichiometry deviation, and is treated as the variable expressing the diffusion.

Figure 2 shows the basic schematic of a two phase

Stefan problem. Material properties are defined in tables 1 and 2. The Q term is an undefined source term that can include a mass or a heat source term. The heat equation and diffusion equation must be satisfied in both the liquid (l) and the solid (s) phases independently. Since this is a binary system with potentially large concentration gradients, the heat of mixing must also be considered in the heat equation. The contribution of the heat of mixing to the total heat flux is shown in equation 1.

$$q_{total} = q_{conduction} + \frac{\partial h}{\partial x} \cdot J_x \tag{1}$$

where $h = h(T, x)$ is the specific enthalpy and $J_x$ is the flux of excess oxygen.

The temperature profile in the sample is continuous across the boundary, however there is a discontinuity in the heat flux as a result of the movement of the boundary over time. The temperature at the boundary is constrained to a specified melting temperature, depending on the local stoichiometry. The oxygen profile is discontinuous at the boundary if the O/U ratio is not 2, i.e., the sample is non-stoichiometric. Such is the case for defective fuel partially oxidized by the coolant. In this case, the oxygen concentration is equal to the liquidous concentration in the liquid phase, and the solidous concentration in the solid phase. The assumption of local equilibrium at all times implies that, at the boundary, the melting temperature and solidous and liquidous concentrations are all interrelated by the phase diagram. These constraints are summarized in reference [2]. The relationship of these variables must be enforced throughout the modelling process.

With these assumptions, the movement of the phase change front may be determined by a mass/energy balance across this region, accounting for the effects of the boundary movement. It is important to note that the rate of the phase front movement is independent of any motion of the liquid phase. The rate of interface movement is the rate of melting/fusion for positive values and conversely the rate of solidification for negative values.

## Temperature

Consider an idealized two phase region as in Figure 1. The normal direction, $\hat{n}$ is defined as going from the liquid to the solid, in accordance to the convention of [3].

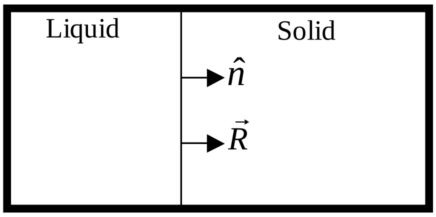

Figure 1: By convention, $\hat{n}$ is the unit normal defined as pointing from the liquid to the solid and $R$ is the rate of fusion.

From first principles we know that the heat balance is:

$$\dot{h}_{in} - \dot{h}_{out} = \dot{h}_{stored} \tag{2}$$

where $\dot{}$ indicates the time derivative.

Thermal energy is stored in the material via a change of phase from solid to liquid, and so a term to account for this must be included. This is the *latent heat of fusion* and is represented mathematically by $\dot{h}_{stored} = \rho H_f R$ where $H_f$ is the latent heat of fusion, $R = \vec{R} \cdot \hat{n}$ is the rate of fusion, and $\rho$ is the density of the phase being changed.

If we take $\dot{h}_{in} = q_l$, $\dot{h}_{out} = q_s$ and $\dot{h}_{stored}$ as defined above, equation 2 may be written as:

$$q_l - q_s = \rho H_f R \tag{3}$$

Now with equation 1, $q_{conduction} = -k\hat{n} \cdot \nabla T$ and $J_x = -D\hat{n} \cdot \nabla x$, equation 3 can be written in its most basic form as:

$$\hat{n} \cdot \left( -k_l \nabla T_l - \frac{\partial h}{\partial x} \cdot D_l \nabla x_l \right) - \hat{n} \cdot \left( -k_s \nabla T_s - \frac{\partial h}{\partial x} \cdot D_s \nabla x_s \right) = \rho H_f \hat{n} \cdot \vec{R} \tag{4}$$

where $k$ is the thermal conductivity, D is the diffusion coefficient and the subscripts $_l$ and $_s$ refer to the liquid and solid, respectively.

## Diffusion

The concentration of excess oxygen, $x$, can be treated in the same way as the energy is treated above. Equation 2 becomes:

$$\dot{x}_{in} - \dot{x}_{out} = \dot{x}_{stored} \tag{5}$$

where $x$ is the concentration of excess oxygen.

The storage term in equation 5 becomes the increase in the species concentration along the solidus and liquidus lines as given by $\dot{x}_{stored} = (x_l - x_s)R$. Expanding the diffusive flux, equations 6 and 7 can now be written for the diffusion of one species in another:

$$J_l - J_s = (x_{liquidus} - x_{solidus})R \tag{6}$$

$$\begin{aligned}\hat{n} \cdot (-D_l \nabla x_l) - \hat{n} \cdot (-D_s \nabla x_s) \\ = (x_{liquidus} - x_{solidus})\hat{n} \cdot \vec{R}\end{aligned} \tag{7}$$

# The melting $UO_{2+x}$ experiment

The current model is being compared with an experiment done by D. Manara at the Institute for Transuranium Elements in Karlsruhe, Germany. In multiple papers, he outlines the experimental procedure for obtaining measurements of the melting transition in non-stoichiometric $UO_2$[4]. The results of these experiments are published and compared with a computer model developed at the ITU [5]. These papers are used to guide and verify the development of the modelling technique in this work.

In the Manara experiment, a prepared sample of $UO_{2+x}$ is held suspended in a high pressure buffer gas to suppress the possible effects of $UO_3$ evaporation. The sample is heated on one side with a combination of two lasers whose beams are homogenized by random mixing over a long fiber optic cable. One laser is used at lower power to slow and condition the cooling rate to prevent undercooling. This effect would complicate the modelling procedure. The other laser is used at higher intensity to heat the surface of the sample and induce melting. The model described in Manara's work [6] is one dimensional in depth for a flat sample of thickness L with heat/mass transfer in the $z$ direction. This is taken as a starting point for the current model development.

Thermal boundary conditions for the heat transport inside the sample include total laser heating, radiative heat transfer, conductive heat transfer to the buffer gas and vaporization of the sample. The front boundary condition describes the heat source as a combination of all these terms and is given in equation 8. The rear condition does not include incident energy or vaporization due to the low temperatures, and is given in Equation 9.

$$\begin{aligned}q_{z=0} = A_l Q_l(t) - \epsilon(T)\sigma \cdot (T^4 - T^4_{ambient}) \\ - q_{gas} - \Delta H_{vap}\phi_{vap}\end{aligned} \tag{8}$$

$$q_{z=L} = -\epsilon(T)\sigma \cdot (T^4 - T^4_{ambient}) \tag{9}$$

$A_l$ is the material absorption coefficient, $Q_l(t)$ the input laser power, $\epsilon(T)$ the material emissivity, $\sigma$ the Stephan-Boltzmann constant, $q_{gas}$ is the conductive heat flux into the buffer gas, $\Delta H_{vap}$ is the specific evaporation heat and $\phi_{vap}$ is the evaporation rate determined as below.

To best reproduce the effects of the buffer gas on the heat equation, an additional domain was added to the model on either side of the $UO_{2+x}$ sample. The heat and diffusion equations are solved simultaneously with the $UO_{2+x}$ model and coupled to the surface temperature. The buffer gas domain is 1 mm thick in accordance with the Manara experimental apparatus. The gas is considered to be stagnant due to short time scale of the experiment; therefore convective effects are not included.

The temperature of the gas was set equal to the temperature of the sample at the surface. This effectively imposed the buffer gas conductive heat loss onto the sample surface. Therefore, $q_{gas}$ in equation 8 is not calculated explicitly. The other boundary of the gas domain is insulative.

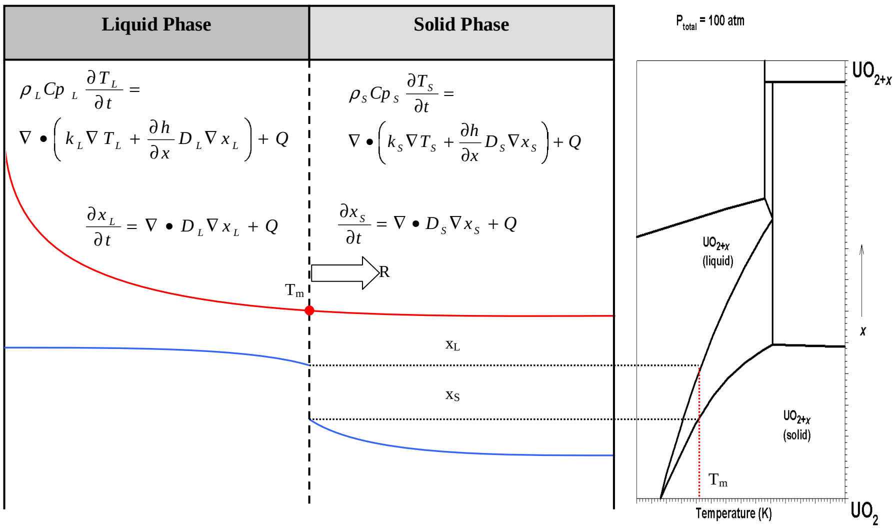

Figure 2: (Left) Schematic of the Stefan problem showing the governing partial, differential equations. (Right) A schematic U-O phase diagram at high temperature

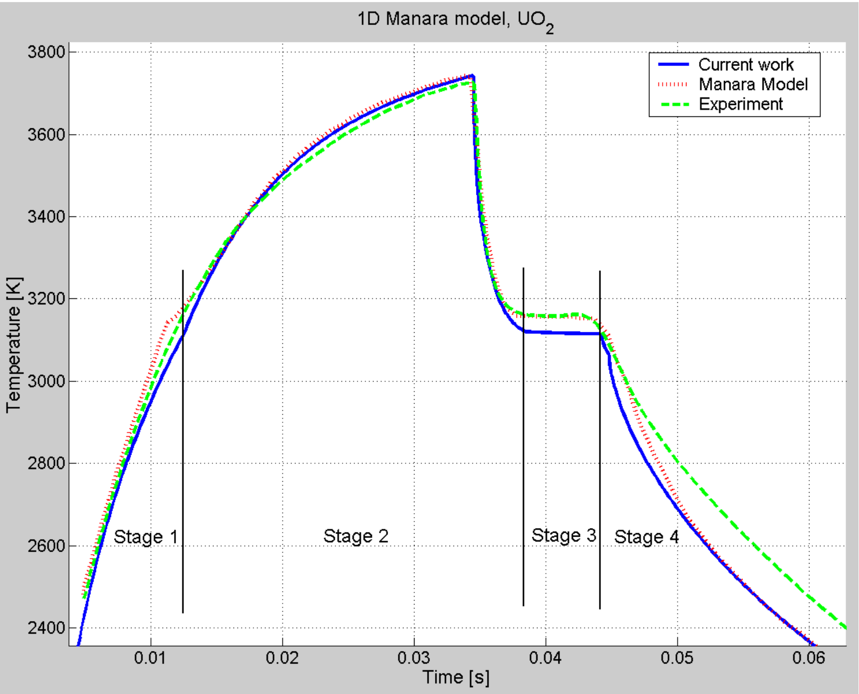

Figure 3: Surface temperature vs. time for $UO_2$.

The partial pressure of $UO_3$ vapour above the liquid $UO_2$ can be obtained through correlations with the sample surface temperature. This partial pressure was converted to a concentration of $UO_3$ in the He gas through the ideal gas law. The vapour is allowed to diffuse from the sample surface into the buffer gas using a classical diffusion equation in the gas domain. Since the partial pressure above the surface must be maintained, this requires addition vapourization from the sample surface. Thus, the evaporation rate $\phi_{vap}$ is determined as the diffusive flux of $UO_3$ vapour at the sample surface.

For the buffer gas, the thermal conductivity used is:

$$k_{He} = 0.152 \left(\frac{T}{300}\right)^{.71} [7] \qquad (10)$$

and the diffusion coefficient of $UO_3$ vapour in He is estimated from the Chapman-Enskog kinetic theory:

$$D_{UO_3He} = 0.001858T^{3/2} \frac{\sqrt{1/MHe + 1/MUO_3}}{P\sigma^2_{HeUO_3}\Omega_D} \qquad (11)$$

The effect of the evaporation of $UO_3$ from the surface was later found to be negligible. Therefore the uncertainty in the estimate of $D_{UO_3He}$ is of minor consequence.

Throughout the experiment, it was assumed that the surface temperature is much lower than the boiling point of $UO_2$. Thus, while evaporation contributes to heat loss, negligible material is lost to the buffer gas by ebullition. Therefore, the diffusion boundary condition is insulating.

$$J_{z=0,L} = 0 \qquad (12)$$

As in the ITU model, the laser power profile $Q_l(t)$ is set to obtain the maximum temperature observed in the experiment.

# Material properties

Material properties were taken mostly from the Fink [8] review, and are summarized in tables 1, 2 and 3. The values are reported for 95% theoretical density $UO_2$. The liquid thermal conductivity used is $3.0\frac{W}{mK}$ instead of the recommended value of $2.5 \pm 1\frac{W}{mK}$ [8, 9]. This is done to better match the length of the plateau observed in the experiment.

The absorption coefficient recorded has a temperature dependence modification to the value recommend by Bober and Fink, $0.8 \pm 20\%$ [8, 10]. This was motivated by the trend in the absorption coefficients observed by Bober in his experiment. Figure 4 shows this trend for four different wavelengths. The average of this trend was taken, normalized and fit with a third degree polynomial. The results is applied to the recommended absorption coefficient. The total change in the value is within the given uncertainty.

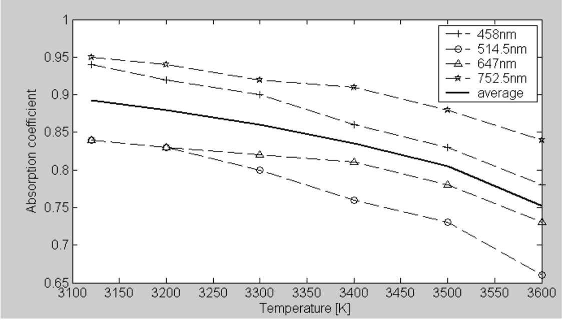

Figure 4: Absorption coefficient as a function of Temperature

The liquidus and solidus lines were obtained from the phase diagram in reference [11].

In summary, this model requires the solution of several coupled non-linear partial differential equations over time. Heat and diffusion equations are solved in the liquid and solid phases as shown in Figure 2. The relationship between the melting temperature, solidus and liquidus concentrations as described by the U-O binary phase diagram, as well as equations 4 and 7 must be satisfied at the boundaries between solid and liquid phases. At the front and rear surface of the sample, the thermal boundary condition is given by equations 8 and 9 respectively, which

| Symbol | Description | Value |
|---|---|---|
| $\sigma$ | Stefan-Boltzmann constant | $5.670 \cdot 10^{-11} \frac{kJ}{K^4 m^2 s}$ |
| $H_f$ | Latent heat of fusion [21] | $74.8 \frac{kJ}{mol}$ |
| $r_o$ | Radius of solute Oxygen atom [22] | $1.4 \cdot 10^{-10} m$ |

Table 3: Contants

involves the solution of heat and diffusion equations in the buffer gas. Material properties of solid and liquid $UO_{2+x}$ are given in tables 1 and 2 respectively and are generally calculated based on $T$ and $x$.

Since this problem is time dependent, the initial conditions must be given. The sample starts at a uniform stoichiometry and temperature. The initial temperature used in the results presented here is 700K and is fairly arbitrary. The stoichiometry changed for each simulation. The model is run in a sequence of four stages, as described below. Upon the creation of a liquid or solid phase, the $x$ in that region is initialized to the liquidus/solidus concentration for that temperature.

This model is solved using Comsol Multiphysics 3.2, a popular commercial software package that uses the Finite Element Method.

## 1-D simulation results

Figure 3 shows the simulation results for the 1 dimensional model using stoichiometric $UO_2$. The temperature of the surface of the sample is recorded over time and compared to the experimental data obtained by Manara, and the model developed at ITU. The thermogram may be divided into four stages:

1. The sample is completely solid and being heated rapidly by the combined heating and conditioning lasers.

2. The surface temperature has passed the melting temperature. There are now two phases present; a liquid phase near the surface of the sample, and the bulk solid phase. The liquid phase grows with time until a maximum temperature is reached. After this point the heating laser is turned off and the sample cools rapidly until the free surface temperature reaches the melting temperature again. Concurrently, the liquid region is resolidifying against the underlying solid.

3. The free surface liquid temperature meets the melting temperature and starts to solidify. Solidification now advances from both the surface and the bulk into the liquid. The conditioning laser is used to prevent undercooling of the sample. As the liquid solidifies, the latent heat is released, which, combined with the conditioning laser, helps to keep the temperature at the surface approximately constant. This produces the observed plateau in temperature until all the liquid is resolidified.

4. The liquid phase is now completely solidified and there is only the solid phase remaining. The temperature slowly becomes uniform over the sample. There is a kink in the temperature profile when the conditioning laser is turned off.

Since the sample in Figure 3 is stoichiometric, the melting occurs congruently. This is not the case for non-stoichiometric fuels. Figures 5(a) and 5(b) show the thermogram for $UO_{2.01}$ and $UO_{2.03}$. One can immediately see the effects of non-stoichiometry in the refreezing process. The solidification plateau is now curved and has a bump before solidification is completed. These effects can be accounted for by the changes in oxygen concentration due to the phase change process. Figure 6(a) shows temperature-depth profiles for four times. The presence and progress of the liquid phase can be clearly seen as the dotted line advances into the sample. The computed profile at 40.4 ms shows the liquid phase surrounded by solid phase advancing from the free surface and from the bulk.

Figure 6(b) shows the deviation from stoichiometry at the same time as the temperature in Figure 6(a). In accordance with the U-O binary phase diagram[11], $x$ in the liquid phase must be equal to the liquidous concentration at the melting temperature. Since this is greater than $x$ in the solid phase, additional oxygen must be rejected from the solid into the liquid phase at a rate that is proportional to the rate of fusion. This creates an outward flux of oxygen from the solid phase, which serves to lower the local

| Symbol | Description | Value | ± % |
|---|---|---|---|
| $A_l$ | Absorbtion coefficient [10, 8] | 0.7 | 20 |
| $\epsilon$ | Emissivity [8, 12] | 0.85 | 1 |
| $k$ | Thermal conductivity [13] | $\frac{10^2}{7.5408+17.692t+3.614t^2} + \frac{6400 \cdot 10^{-16.35/t}}{t^{5/2}} \frac{W}{m\ K}$ | $10 - 20$ |
| $C_p$ | Heat capacity [11] | $52.1743 + 45.8056x + (87.951 \cdot 10^{-3} - 7.3461 \cdot 10^{-2}x)T + (1-x)(-84.2411 \cdot 10^{-6}T^2 + 31.542 \cdot 10^{-9}T^3 - 2.6334 \cdot 10^{-12}T^4) - (0.713910 + 29509x)T^{-2} \frac{J}{molK}$ | $4 - 13$ |
| $\rho/\rho(273)$ | Density expansion[8, 14] | $9.97 \cdot 10^{-1} + 9.08 \cdot 10^{-6}T - 2.71 \cdot 10^{-10}T^2 + 4.39 \cdot 10^{-13}T^3 \frac{Mg}{m^3}$ for $273 < T < 923$<br>$9.97 \cdot 10^{-1} + 1.18 \cdot 10^{-5}T - 2.43 \cdot 10^{-9}T^2 + 1.22 \cdot 10^{-12}T^3 \frac{Mg}{m^3}$ for $923 < T < 3120$ | 1<br>1 |
| $P_{sat}$ | Saturated vapour pressure [15, 16] | $10^{-31284/T+7.616}$ MPa | $-40/+60$ |
| $D_s$ | Diffusion of Oxygen in UO2 [17] | $2.5e^{(}-16400/T)\frac{cm^2}{s}$ | |

Table 1: Solid property values. $t = T/1000$, $\Delta T = T - 3120$

| Symbol | Description | Value | ± % |
|---|---|---|---|
| $A_l$ | Absorbtion coefficient* | $0.8 \cdot (-1.013t^3 + 9.74t^2 - 31.42t + 34.98)$ | |
| $\Delta H_{vap}$ | Heat of evaporation [8, 18] | $516.382 - 0.022946T \frac{kJ}{mol}$ | |
| $\epsilon$ | Emissivity [8, 19] | $1 - 0.16096e^{-3.7897 \cdot 10^{-4}\Delta T) - 3.2718 \cdot 10^{-7}\Delta T^2}$ | 3 |
| $k$ | Thermal conductivity* | $3.0 \frac{W}{m\ K}$ | |
| $P_{sat}$ | Saturated vapour pressure [8, 18] | $10^{15.961 - 26974/T - 2.76 \log_{10} T}$ MPa | $-40/+60$ |
| $C_p$ | Heat capacity [8] | $0.25136 + \frac{1.3288 \cdot 10^9}{T^2} \frac{J}{molK}$ | $10 - 25$ |
| $\rho$ | Density expansion[8, 18] | $8.860 - 9.285 \cdot 10^{-4} \cdot \Delta T \frac{Mg}{m^3}$ | $2 - 4$ |
| $D_l$ | Diffusion of Oxygen in UO2 [20] | $\frac{k_B * T}{6\pi r_O \eta} \cdot 10^7 \frac{cm^2}{s}$ | |
| $\eta$ | Viscosity of molten UO2 [8] | $.988e^{4620/T} mPa \cdot s$ | 25-50 |

Table 2: liquid property values. $t = T/1000$, $\Delta T = T - 3120$. *refer to text.

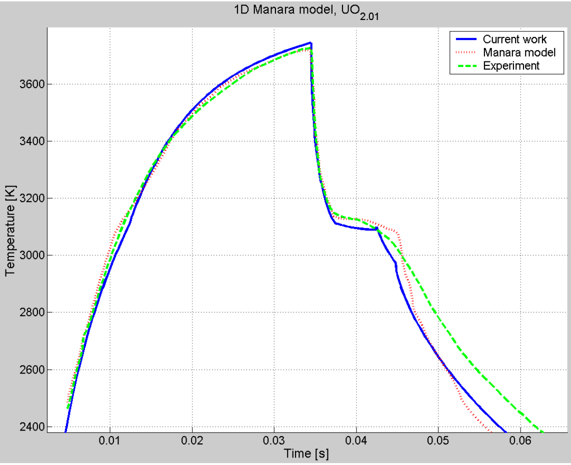

(a) $UO_{2.01}$

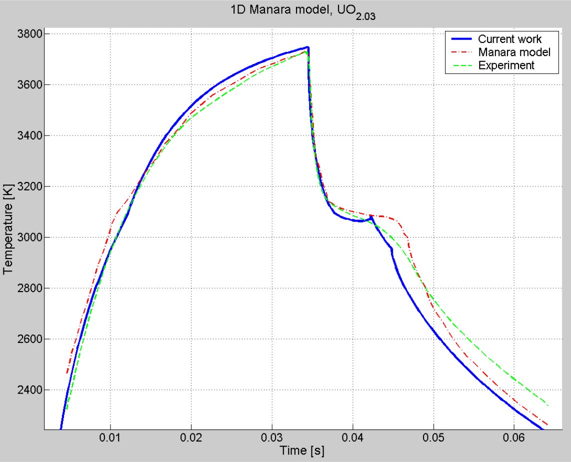

(b) $UO_{2.03}$

Figure 5: Surface temperature vs. time.

concentration of oxygen in the solid. This, in turn, lowers the corresponding liquidous concentration. Simultaneously, the melting temperature changes with the local stoichiometry. This consistent set of conditions arises from the interrelations depicted on the phase diagram. The resulting profile can be seen at a time of 34 ms.

Upon the onset of freezing, the aforementioned sequence is reversed. The solid being created is at a lower stoichiometry than the liquid, resulting in an enrichment of the oxygen content in the liquid phase. Time 40.4 ms shows both solidification fronts advancing into the liquid, and the effect of this on the $x$ in the liquid. One can deduce that the last liquid is highly enriched in oxygen before solidifying. This

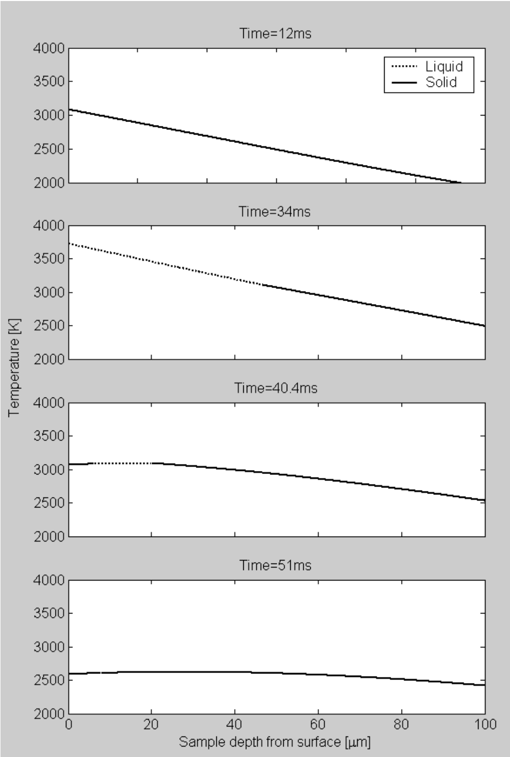

(a) Temperature

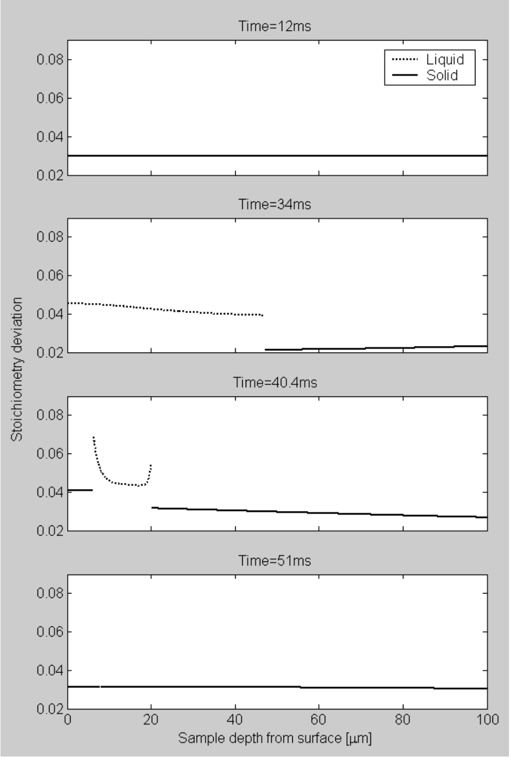

(b) Stoichiometry

Figure 6: Depth profiles for $UO_{2.03}$

creates large oxygen diffusive flux as the material homogenizes. The heat of mixing now contributes largely to the heat flux, and creates the bump seen in Figure 5(b) at time 42 ms. The large concentration gradient relaxes quickly at the high temperature and small distances and a profile similar to the original constant value is quickly established.

# Conclusions

The results obtained from the 1D simulation give assurance that the developing mathematical concept and implementation is sound. The expansion of this model into 2D is expected to smooth the complex freezing process to better match the experimental data. Material properties may be adjusted within the experimental uncertainty to better fit the data. This work has direct application to describing the centerline melting phenomenon in operating defective fuel elements with the presence of hyperstoichiometric (i.e., oxidized) fuel.

# Acknowledgements

This work was funded by a Collaborative Research and Development grant from the Natural Sciences and Engineering Research Council of Canada [NSERC] and is being performed at The Royal Military College of Canada. I would like to thank my supervisors Dr. Lewis and Dr. Thompson for their guidance, advice and support. Also, Dr. Manara for the advice and information he provided me.

# References

[1] J. Donea et al.The Encyclopedia of Computational Mechanics Vol. 1 (Wiley, 2004) chap. 14: Arbitrary Lagrangian-Eulerian methods, pp. 413–437.

[2] F. Akbari, B. Lewis and W. Thompson, CANDU IX Fuel conference proceedings, 2005.

[3] S. Kou, Transport Phenomena and Materials Processing (John Wiley & Sons, Inc., 1996).

[4] D. Manara et al., Journal of Nuclear Materials 342 (2005) 148.

[5] V. Atrazhev and M. Brykin, Numerical simulation of melting and solidification of bindary mixtures in laser heating pulses (non-congruent phase transition solid-liquid), Study Contract N. 17644-2001-03F1SC KAR RU Final Report (ITU).

[6] D. Manara, Melting Transition Measurements in Uranium Dioxide, PhD thesis, University of Warwick, 2004.

[7] N.B. Vargaftik and Y.D. Vasilevskaya, Journal of Engineering Physics 42 (1982) 296.

[8] J.K. Fink, Journal of Nuclear Materials 279 (2000) 1.

[9] H.A. Tasman, Thermal conductivity of liquid $\mathrm{uo}_2$, 1988.

[10] M. Bober, J. Singer and K. Wagner, Eighth Symposium on Thermophysical Properties Vol. II, pp. 234–244, Gaithersburg, MD, 1981, ASME, New York, 1982.

[11] B. Lewis et al., Journal of Nuclear Materials 328 (2004) 180.

[12] J.H. Harding, D.G. Martin and P.E. Potter, Thermophysical and thermochemical properties of fast reactor materials, 1989.

[13] C. Ronchi et al., Journal of applied physics 85 (1999) 776.

[14] D.G. Martin, Journal of Nuclear Materials (1988) 94.

[15] I.N.S.C.M.P. Database, Material properties of uranium dioxide (uo2), Internet document: http://www.insc.anl.gov/matprop/uo2/.

[16] M. Tetenbaum and P.D. Hunt, Journal of Nuclear Material 34 (1970) 86.

[17] J. Meachen, Nuclear Energy (1989) 221.

[18] W. Breitung and K.O. Reil, Nucl. Sci. Eng. 101 (1989) 26.

[19] C.L. Fink, private conversation to j. k. fink.

[20] B. Lewis et al., Journal of Nuclear Material 227 (1995) 83.

[21] J.K. Fink, M.G. Chasanov and L. Leibowitz, Journal of Nuclear Materials 102 (1981) 17.

[22] Handbook of Chemistry and Physics (CRC Press, 1975).